

Far-ultraviolet investigation into the galactic globular cluster M30 (NGC 7099): II. Potential X-ray counterparts and variable sources

Santana Mansfield^{1*}, Andrea Dieball¹, Pavel Kroupa^{1,2}, Christian Knigge³, David R. Zurek⁴, Michael Shara⁴, and Knox S. Long⁵

¹Helmholtz-Institut für Strahlen- und Kernphysik (HISKP), Universität Bonn, Nußallee 14-16, D-53115 Bonn, Germany

²Astronomical Institute, Faculty of Mathematics and Physics, Charles University in Prague, V Holešovičkách 2, CZ-18000 Praha, Czech Republic

³School of Physics and Astronomy, University of Southampton, Highfield, Southampton SO17 1BJ, UK

⁴Department of Astrophysics, American Museum of Natural History, New York, NY 10024, USA

⁵Space Telescope Science Institute, 3700 San Martin Drive, Baltimore, MD 21218, USA

Accepted XXX. Received YYY; in original form ZZZ

ABSTRACT

We present a far-ultraviolet (*FUV*) study of the globular cluster M30 (NGC 7099). The images were obtained using the Advanced Camera for Surveys (ACS/SBC, F150LP, *FUV*) and the Wide Field Planetary Camera 2 (WFPC2, F300W, *UV*) on board the *Hubble Space Telescope* (*HST*). We compare the catalogue of *FUV* objects to ten known X-ray sources and find six confident matches of two cataclysmic variables (CVs), one RS CVn, one red giant with strong *FUV* emission and two sources only detected in the *FUV*. We also searched for variable sources in our dataset and found a total of seven blue stragglers (BSs), four horizontal branch (HB) stars, five red giant branch stars, 28 main sequence stars and four gap objects that demonstrated variability. One BS star is a known W-UMa contact binary, one of the gap objects is a known CV identified in this work to be a dwarf nova, and the three other gap sources are weak variables. The periods and positions of two of the variable HB stars match them to two previously known RR Lyrae variables of types RRab and RRc.

Key words: ultraviolet: stars – stars: variable: general – globular clusters: individual: M30 (NGC 7099) – novae, cataclysmic variables – horizontal branch – techniques: photometric

1 INTRODUCTION

The high density of stars in the cores of globular clusters allows frequent interactions which produces various exotic sources such as blue straggler (BS) stars which are located at brighter magnitudes in the colour magnitude diagram (CMD) than the main sequence (MS) turnoff. BS stars are typically thought to have higher masses than MS stars, by gaining mass from a companion (McCrea 1964), or from a direct collision (Hills & Day 1976), in order to remain in the location of the zero-age main sequence (ZAMS) while single MS stars of similar masses have turned off to become red giants. Other exotic sources include binary systems such as cataclysmic variables (CVs; a white dwarf (WD) star accreting mass from a companion), X-ray binaries and millisecond pulsars (MSPs, Shara & Hurley 2006; Ivanova et al. 2008; Hong et al. 2016).

CVs and low-mass X-ray binaries (LMXBs; a neutron star or black hole accreting material from a low-mass companion), are faint at optical wavelengths and not easily detectable in globular clusters as they are surpassed by the large number of MS stars that shine brightly in the optical. Instead, we search for these exotic sources in the ultraviolet and X-ray wavelengths. Since the accretion of material in these binary systems results in very hot temperatures in the accretion disk, as well as when material falls onto the surface of the compact

object, the spectral energy distribution of this hot emission peaks in the far-ultraviolet (*FUV*) or X-ray wavelengths. Since the surfaces of the numerous MS and red giant branch (RGB) stars in globular clusters do not reach such high temperatures, they are faint at these wavelengths and the cluster core appears much less crowded. By taking observations in the ultraviolet, we can more easily detect and identify such exotic sources.

For the first part of this investigation (Mansfield et al. 2022, hereafter Paper I), we performed the photometry of ultraviolet observations of the globular cluster M30 (NGC 7099) and presented a *FUV* – *UV* CMD and an analysis of the radial distributions of the different stellar populations. A more detailed overview of M30 and the previous studies on this cluster can be found in Paper I. We also presented an ultraviolet catalogue of sources¹. In this present work we continue our investigation into the properties of M30 and compare the positions of the sources detected in the ultraviolet to the locations of the known X-ray sources in M30. In this work we also perform a variability study using the *FUV* exposures to find active binary systems in M30, including those in the vicinity of X-ray sources.

Stars can exhibit brightness variability due to the orbit of a binary (or multiple) system, structural processes within single stars which

¹ <http://vizier.u-strasbg.fr/viz-bin/VizieR?-source=J/MNRAS/511/3785>

* Email: smansfield@astro.uni-bonn.de

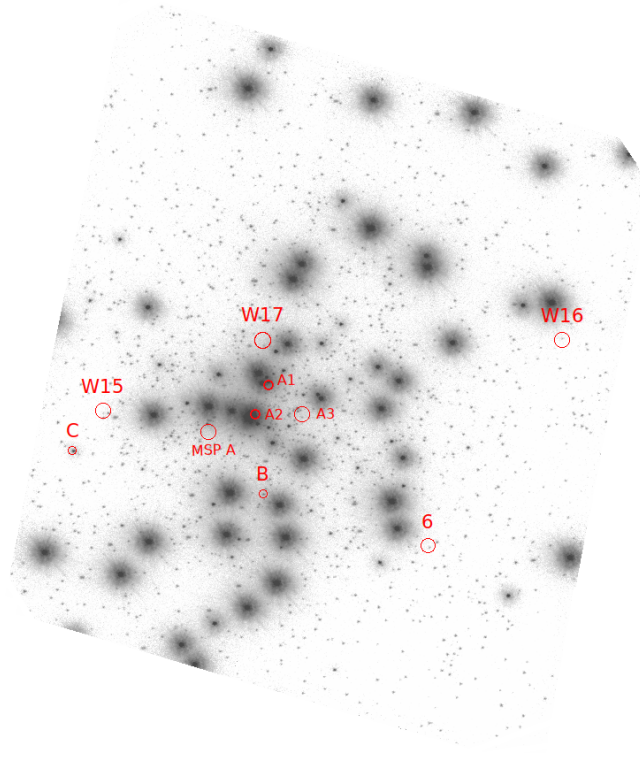


Figure 1. Positions of the 10 X-ray sources listed in Table 1, seen as red circles with sizes proportional to their positional uncertainties, superimposed onto the *FUV* master image of M30. North is up, east is to the left and the image spans $34.6'' \times 30.8''$.

generate pulsations, or from interactions between binary members such as mass transfer. For example, the emission from a hot accretion disk in a CV system, as well as the fall of material onto the surface of the WD, can produce strong variability which helps to distinguish CVs from isolated WDs. Investigating brightness fluctuations allows for precise stellar identification within the population groups. For instance, within M30, seven RR Lyrae variables have been observed on the horizontal branch (HB) in the optical and infrared (Pietrukowicz & Kaluzny 2004; Kains, N. et al. 2013), and since Zurek et al. (2016) saw brightness variability on the HB in the *FUV* for NGC 1851, a variability study of M30 in the *FUV* will be valuable to find other potential RR Lyrae stars on the horizontal branch of M30, as well as possible CV candidates.

M30 also contains a number of X-ray sources which indicate exotic binary systems. Lugger et al. (2007) detected 13 X-ray sources that were also found by Zhao et al. (2020), who discovered an additional 10 sources, based on observations with *Chandra* ACIS-S. Some of these sources are thought to be CVs, and one is likely a quiescent low-mass X-ray binary (qLMXB). Two milli-second pulsars were also found in M30 by Ransom et al. (2004).

The observations and coordinate transformations used for this investigation are described in Sect. 2. The potential ultraviolet counterparts to the X-ray sources and their locations in the *FUV* – *UV* CMD are described in Sect. 3. The variable sources are described in Sect. 4, followed by a summary in Sect. 5.

2 DATA PROCESSING

2.1 Photometry

The far-ultraviolet (*FUV*) data was obtained with the Advanced Camera for Surveys (ACS) on board the *HST*, using the Solar Blind Channel (SBC) and the F150LP filter. The *UV* data was acquired using the Wide Field Planetary Camera 2 (WFPC2) and the F300W filter, which was also on board the *HST*. These were both part of the program GO-10561 (PI: Dieball) and were taken using 15 orbits distributed over three visits, from the 29th May to the 9th June 2007. The SBC has a field of view of $34.6'' \times 30.8''$ and a pixel scale of $0.034'' \times 0.030'' \text{ pixel}^{-1}$. Sixty-four images were taken, each with an exposure time of 315 s, resulting in a total exposure time of 20160 s. The WFPC2 consists of four cameras, the three Wide Field Cameras (WFCs) each with a field of view of $50'' \times 50''$, and the Planetary Camera (PC) with a field of view of $34'' \times 34''$, and a pixel scale of $0.046'' \text{ pixel}^{-1}$. As the PC was centred on the cluster core and the region observed for the *FUV* imaging, only the exposures from this camera were used in this work. Twenty-four images were taken with a total exposure time of 12000 s. The observations, image processing and data reduction are described in detail in Paper I. Out of 1934 sources detected in the *FUV*, 1569 have *UV* counterparts, including 1218 MS stars, 41 horizontal branch (HB) stars, 47 blue stragglers (BS), 185 RGB stars and 78 WD/Gap objects (sources blueward of the MS and with $FUV \gtrsim 19 \text{ mag}$).

The optical data used in this work is the catalogue from Guhathakurta et al. (1998), the exposures of which were also taken with the WFPC2 on board the *HST* (program GO-5324, PI: Yanny). Eight exposures were taken on 31st March 1994, two using the F336W filter with 100 s exposure time, two using the F439W filter and 40 s exposure time and four using the F555W filter with 4 s exposure times. The data was accessed from VizieR².

2.2 X-ray coordinate transformation

Lugger et al. (2007) found 13 X-ray sources within the half-mass radius of M30 ($1.15'$, Harris 1996) using *Chandra* ACIS-S. In order to check the positions of these sources against our ultraviolet dataset, we use the astrometric reference star adopted by Guhathakurta et al. (1998), a red giant (their source #3611), which in our catalogue is ID366. From our dataset, the position of this star is:

$$\alpha = 21^{\text{h}}40^{\text{m}}22^{\text{s}}.31, \quad \delta = -23^{\circ}10'40''.13 \quad (\text{J2000.0}) \quad (1)$$

which has a shift of $\Delta\alpha = +0.02''$, $\Delta\delta = +0.53''$ from the position of $\alpha = 21^{\text{h}}40^{\text{m}}22^{\text{s}}.29$, $\delta = -23^{\circ}10'39''.60$ given by Lugger et al. (2007) (and also a relatively small shift of $\Delta\alpha = -0.004''$, $\Delta\delta = +0.03''$ to the position of $\alpha = 21^{\text{h}}40^{\text{m}}22^{\text{s}}.314$, $\delta = -23^{\circ}10'40''.10$ reported by Ransom et al. (2004)). This is within the uncertainties of $0.70''$ in the world coordinate system (WCS) for both *HST* and *Chandra*. This positional shift is then applied to the Lugger et al. (2007) X-ray sources in order to match to our dataset. These 13 sources were also detected by Zhao et al. (2020) as well as an additional 10 sources within the updated half mass radius of $1.03'$ (Harris 2010). By comparing the coordinates given for the 13 sources discovered by Lugger et al. (2007) to those of Zhao et al. (2020), an additional shift can be applied to the new 10 sources to match them to our dataset. Out of the 23 total sources, 10 are within the *FUV* field of view and are marked in Fig. 1. After comparing the datasets, we find six confident

² <https://vizier.cds.unistra.fr/viz-bin/VizieR?-source=J/AJ/116/1757>

Table 1. The positions and distances of the potential counterparts to the X-ray sources and their ultraviolet photometric quantities as found in this study. The radius r in Column 2 is the distance of the X-ray source from the centre of the cluster, and the distance of the potential counterpart to the X-ray source is given in Column 7. The X-ray sources A1–6 are from [Lugger et al. \(2007\)](#), sources W15–W17 are from [Zhao et al. \(2020\)](#), and the MSP from [Ransom et al. \(2004\)](#).

ID _{X-ray}	r [arcsec]	P_{err}^a [arcsec]	ID _{FUV}	RA [h:m:s]	Dec [°:′:″]	Distance [arcsec]	Err ^b	Type	<i>FUV</i> [mag]	<i>FUV-UV</i> [mag]
A1	1.312	0.24	ID272	21:40:22.16	-23:10:45.85	0.238	0.992	BS	17.170 ± 0.004	-0.676 ± 0.006
A2	1.064	0.24	ID283	21:40:22.22	-23:10:47.65	0.078	0.325	BS/RG	17.570 ± 0.013	-0.646 ± 0.016
			ID290	21:40:22.23	-23:10:47.71	0.224	0.933	BS	14.676 ± 0.001	-1.612 ± 0.002
A3	1.599	0.42	ID181	21:40:22.03	-23:10:47.85	0.134	0.319	RG	23.195 ± 0.066	5.677 ± 0.068
			ID187	21:40:22.03	-23:10:47.46	0.289	0.688	RG	22.129 ± 0.034	3.971 ± 0.037
			ID191	21:40:22.04	-23:10:47.51	0.336	0.800	RG	21.549 ± 0.023	5.444 ± 0.024
			ID806	21:40:22.00	-23:10:47.88	0.405	0.964	MS	23.050 ± 0.054	3.801 ± 0.059
B	4.904	0.24	ID1647	21:40:22.18	-23:10:52.17	0.005	0.021	–	21.582 ± 0.026	–
C	11.483	0.24	ID456	21:40:22.96	-23:10:49.74	0.038	0.158	WD/Gap	19.748 ± 0.009	-0.821 ± 0.019
6	11.718	0.41	ID1700	21:40:21.51	-23:10:55.15	0.090	0.220	–	23.256 ± 0.048	–
W15	9.559	0.43	ID449	21:40:22.81	-23:10:47.61	0.292	0.679	MS	22.298 ± 0.029	3.464 ± 0.033
			ID452	21:40:22.83	-23:10:47.88	0.364	0.847	MS	22.453 ± 0.031	3.483 ± 0.035
			ID912	21:40:22.83	-23:10:47.63	0.109	0.253	WD/Gap	23.971 ± 0.071	2.233 ± 0.093
W16	16.672	0.44	ID1029	21:40:20.97	-23:10:43.43	0.108	0.245	RG	23.692 ± 0.060	4.929 ± 0.064
W17	3.843	0.46	ID1681	21:40:22.18	-23:10:43.83	0.297	0.646	–	22.648 ± 0.060	–
MSP A	3.870	0.43	ID1217	21:40:22.39	-23:10:48.35	0.399	0.928	RG	22.272 ± 0.054	3.859 ± 0.057

a) 95% error circle.

b) Characteristic uncertainty, Err = Distance/ P_{err} .

matches: ID283 to A2, ID1647 to B, ID456 to C, ID1700 to 6, ID912 to W15 and ID1029 to W16 (described in detail in Sect. 3). The average distance of these six sources to their X-ray counterparts was 0.148″, which is then used as an additional boresight correction to shift the X-ray catalogue into the *FUV* frame. After this shift the confident matches have an average positional offset of 0.071″.

2.3 Brightness variability

For the variability study, the magnitudes of the individual sixty-four *FUV* exposures were measured using the DAOPHOT task ([Stetson 1987](#)), running under PYRAF ([Greenfield & White 2000](#)). As the individual images are slightly shifted with respect to one another, a specific coordinate list of the sources is first created for each exposure, using the coordinate list of the drizzled master image from [Paper I](#). This list is transformed into individual coordinate lists using the task WCSSTRAN which takes the WCS information from each exposure. Then the DAOPHOT task performs aperture photometry on each exposure using the specific coordinate list. This task was performed without recentering which would measure the magnitude of a nearby bright star if the flux at the target coordinate is faint. Aperture and sky corrections to the measured fluxes are applied using the same method described in [Paper I](#) (Sect. 2.1.2).

3 X-RAY SOURCE MATCHING

3.1 Positional error radii

The X-ray sources are given in Table 1 along with their potential counterparts. The positional 95% error radii P_{err} is included for each X-ray source and is shown in Figs. 1, 3 and 4 as red circles. For the bright sources (> 100 counts, i.e. sources A1, A2, B and C), we calculate P_{err} using the positional uncertainties of the six confident matches and the formula:

$$\sigma_r^2 = \sigma_{RA}^2 + \sigma_{Dec}^2 \quad (2)$$

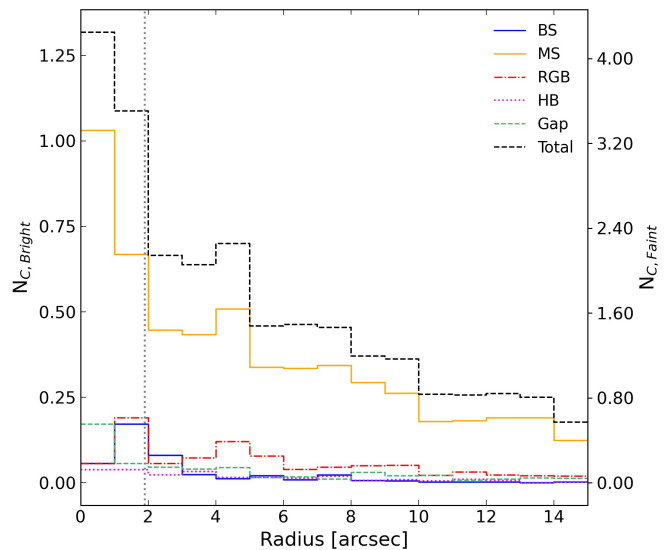


Figure 2. Number of chance coincidences within the error circle for either a bright or a faint X-ray source plotted as a function of radial distance from the centre of the cluster. For a bright source the error radius $A_{err} = 0.18 \text{ arcsec}^2$ is used and for a faint source $A_{err} = 0.58 \text{ arcsec}^2$ is used. The dotted vertical line indicates the cluster core region. The group Total gives the chance of finding any coincidental star in the error radii.

After applying the shifted boresight correction, the rms errors in RA and Dec are 0.076″ and 0.063″ respectively, correlating to 1σ in each of the two directions. A 95% error radii corresponds to 2.45σ and as such the resulting P_{err} for the bright sources is 0.243″.

For the fainter sources, we take the 95% error radii for *Chandra* ACIS-S given by [Zhao et al. \(2020\)](#) and calculated from the individual source count and offset ([Hong et al. 2005](#)). Then all *FUV* sources within P_{err} are marked with blue circles in Figs. 3 & 4 and the locations of these sources in the *FUV-UV* CMD are marked in Fig.

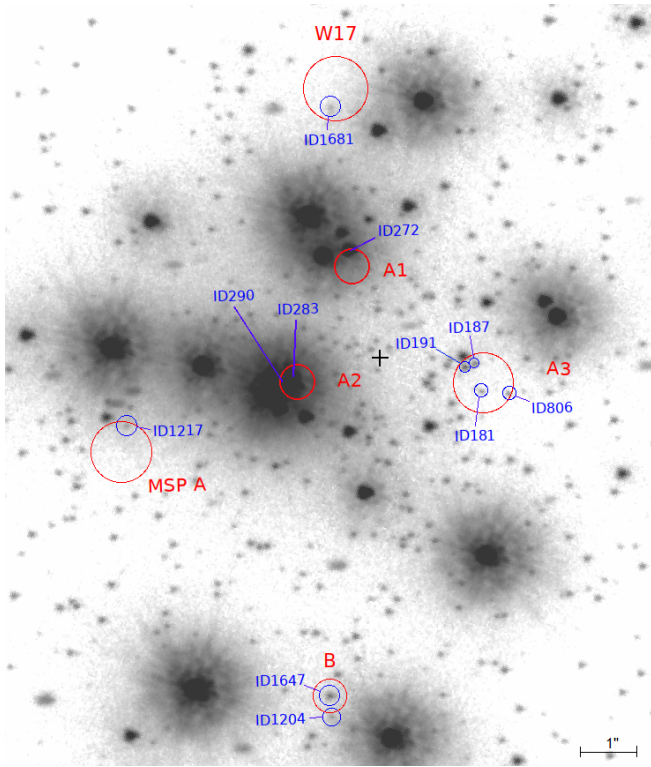


Figure 3. Position of X-ray sources with 95% error radii marked with red circles. The potential counterparts are given in blue. The black cross indicates the centre of the cluster.

5, which includes their optical counterpart locations in the $B - V$ CMD from the [Guhathakurta et al. \(1998\)](#) catalogue. The coordinate transformation to the optical catalogue was described in [Paper I](#).

3.2 Chance coincidences

In the dense core of the cluster there may be stars within the positional error radii that are chance coincidences. To estimate the number of chance coincidences of each stellar population within these radii, we follow the method of [Zhao et al. \(2020\)](#), and split the cluster into concentric annuli with 1 arcsec thicknesses over the 15 arcsec radius contained in our field of view. Assuming the populations are evenly distributed within each annulus, we can then calculate the number of chance coincidences, N_C , using the number of stars in each population in each annulus, N_{tot} , the area of each annulus, A_{ann} , and the area of the 95% positional error radii, A_{err} , in the formula:

$$N_C = N_{tot} \times \frac{A_{err}}{A_{ann}} \quad (3)$$

which we have applied to the bright and faint X-ray sources separately, using the value $A_{err} = 0.18 \text{ arcsec}^2$ for the bright sources and the average value $A_{err} = 0.58 \text{ arcsec}^2$ for the faint sources. The number of chance coincidences found within the error circle for either a bright or a faint X-ray source is shown for each population, as well as the total chance of finding any type of star, is given in Fig. 2. As the area of the 95% positional error is slightly more than three times as large for the fainter X-ray sources, the number of chance coincidences within these radii are also slightly more than triple. Within the very core of the cluster the number of a chance coincidence of any type of

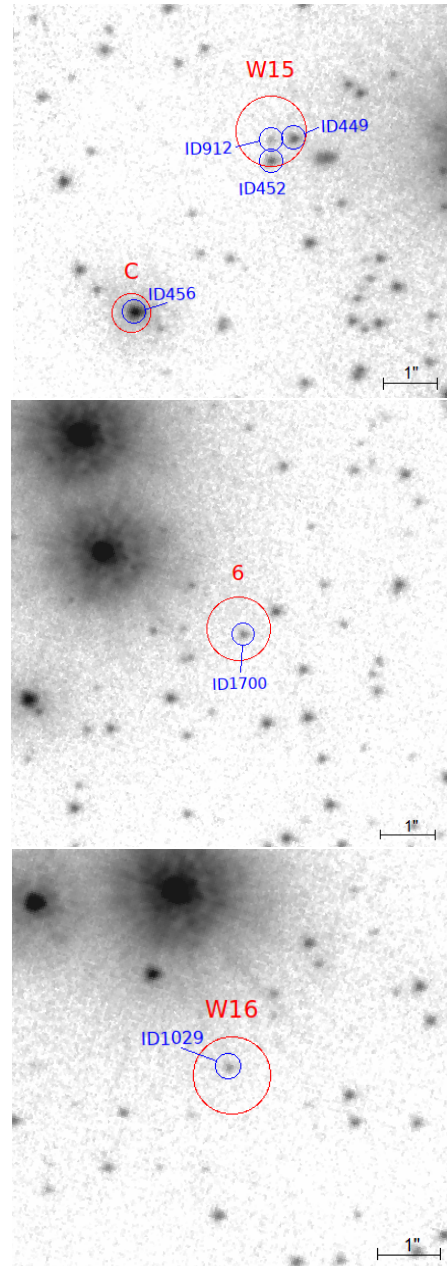


Figure 4. Same as Fig. 3.

star is 1.32 in the area around a bright X-ray source, but drops to an average of 0.52 over the rest of the FUV field of view. The average number of chance coincidences within a faint X-ray error circle is 1.66.

3.3 Cluster membership probability

Some of the ultraviolet sources discussed in this section and also in Sect. 4 have cluster membership probabilities calculated from their proper motions derived from the *Hubble Space Telescope UV Legacy Survey of Galactic Globular Clusters* (HUGS) catalogue ([Piotto et al. 2015](#); [Nardiello et al. 2018](#)). The values for these sources are given in Table 2.

3.4 Potential X-ray counterparts

A total of 16 *FUV* sources are located within the 10 X-ray positional error radii. In order to see if we can already identify a number of these sources as confident matches based on their positions alone, we counted the number of *FUV* sources within the error radii at several small and increasing offsets. Due to the crowding in the centre of the cluster, the total number of *FUV* sources within all 10 error radii remained roughly the same at different offset positions. This indicates that a detailed examination into the characteristics of each potential X-ray counterpart is needed to evaluate the likelihood of associating it with the X-ray source.

3.4.1 Source A1

The X-ray source A1 (Lugger et al. 2007) is thought to be a qLMXB with a neutron star that has either a He atmosphere or a H atmosphere with significant hotspots (Echiburú et al. 2020). As LMXBs in a quiescent state have very reduced or no accretion, they are generally faint at ultraviolet and other wavelengths. Zhao et al. (2020) note that the donor star should be a He WD if the neutron star has a He atmosphere, and it could be a MS star if the neutron star has hotspots which distort the spectrum. Lugger et al. (2007) suggest two MS stars that lie close to the MS turnoff in the optical CMD as possible companions, however they note that the area in the vicinity of A1 is severely crowded. As A1 lies within $2''$ of the cluster centre, the number of coincidental stars within the error radii at this radius is 1.09. From our dataset there is only one potential counterpart that lies on the edge of the error circle for A1, a BS star ID272 with a bright *FUV* magnitude (≈ 17.2 mag), making it one of the brightest BS sources, and it is also relatively bright in the optical, with $V = 18.16$ mag (Guhathakurta et al. (1998), their source #3115). As ID272 is a bright BS star and neither a WD or MS star, it is likely that ID272 is a chance superposition in this dense region of the cluster core, and the true counterpart is too faint to be seen in the *FUV*.

3.4.2 Source A2

Lugger et al. (2007) consider the brightest *FUV* source (#3327 in Guhathakurta et al. 1998, ID290 in this work) as a possible companion to the X-ray source A2 as it sits within $0.50''$ of it. However they note that the crowding in this central region of the cluster (Fig. 3, $N_{C, \text{Bright}} = 1.09$) may mean that a different star may be the companion. From our dataset, the error circle for A2 includes source ID290 at a distance of $0.224''$ which is located in the BS region in the optical CMD (Fig. 5), but has the brightest *FUV* magnitude in this work. Lugger et al. (2007) conclude that this source is likely to be a sub-dwarf B star (sdB) with a WD companion. Yet, as noted by Lugger et al. (2007), not many sdB binaries are known to emit X-ray emission and thus its proximity to A2 could be a chance superposition. There is one other source within the error circle: ID283 at a distance of $0.078''$ from A2. This is an interesting counterpart candidate as in the *FUV* – *UV* CMD it has the position of a bright BS star, however in the optical CMD it is located on the red giant branch. This likely represents a binary system in which the RGB star has overfilled its Roche Lobe and is transferring mass to a compact companion resulting in strong *FUV* emission. CVs undergoing substantial mass transfer appear considerably bluer in the ultraviolet relative to their optical colours. These objects are rare although have been found in other globular clusters (eg. Edmonds et al. 2003). Thus it is likely then that ID283 is the counterpart to the X-ray source A2 and is a CV system with a red giant donor star.

Table 2. Cluster membership probabilities of some of the sources discussed in the text, from the HUGS catalogue (Piotto et al. 2015; Nardiello et al. 2018)

ID	P_{μ} (%)
93	92.6
179	44.2
181	90.2
187	88.5
191	88.5
268	97.5
272	97.1
276	98.0
277	96.9
350	85.1
456	94.3
912	96.7
1029	97.5
1217	95.6
1226	96.7
1230	96.7
1647	90.5
1681	90.5

3.4.3 Source A3

The source A3 was a faint X-ray detection with no optical counterparts proposed by Lugger et al. (2007). In our work there are four sources within the error circle of A3, all with optical counterparts. One MS star lies on the edge of the error circle, ID806, which is located in the MS in both optical and ultraviolet CMDs. As this source does not show significant variability (Sect. 4), this is unlikely to be the counterpart to A3. The number of chance coincidences within the faint X-ray source error radii at this distance from the centre is 1.60 for a MS star and 0.25 for a red giant. Three RGB stars are also in the error circle, making one of these likely to be the correct counterpart. The closest to the X-ray source is ID181 at a distance of $0.134''$, and the other two ID187 and ID191 are at distances of $0.289''$ and $0.336''$ respectively. ID191 shows no variability, however ID181 and ID187 are interesting possibilities as counterparts to A3 as they are both slightly variable stars which could result from instabilities in accretion if they are binary systems. As seen later in Sect. 4, ID187 has a larger standard deviation relative to sources of similar *FUV* magnitude than ID181, and it appears bluer in the ultraviolet CMD relative to the other red giants than the optical CMD. Thus the most likely counterpart to A3 is the variable RGB star ID187, with the closer RGB star ID181 also a possibility.

3.4.4 Source B

Lugger et al. (2007) suggest a faint companion to X-ray source B that lies in the halo of a RGB star and is located on the MS in their infrared CMD, but has blue excess in the ultraviolet and concluded that source B is a potential CV. However no MS star was detected at the location of source B in this present work, and the RGB star ID1204 is located just outside of the error circle for B, at a distance of $0.288''$ and did not show any significant variability. Only one source is located within the error circle for source B, ID1647, which is only detected in the *FUV* and has no *UV* counterpart. At a distance of $0.005''$ from source B, this is the likely counterpart to B and the source which showed blue excess in Lugger et al. (2007). Piotto et al. (2015) and Nardiello et al. (2018) also find a source at this position with a cluster membership probability of 90.5%. The light curve for

a variable WD/Gap object in Sect. 4 where its magnitude in the first observing epoch was ≈ 1.5 mag brighter than in the latter two epochs (Fig. 10). We agree then that ID456 is a CV that is experiencing a dwarf nova event. ID456 is one of the brightest Gap sources, with $FUV \approx 19.7$ mag, however as no source was detected in the optical at this location, and the optical detection limit is $V \approx 22$, this suggests a very faint low mass MS companion. Göttgens et al. (2019) also classify this source (ACS ID 23423) as a CV due to its broad $H\alpha$ and $H\beta$ emission detected with the Multi Unit Spectroscopic Explorer (MUSE, Bacon et al. 2017)

3.4.6 Source 6

One source, ID1700, lies at a distance of $0.090''$ from X-ray source 6 from Lugger et al. (2007) and is detected in the FUV but is not seen in the UV . Due to the detection limit of $UV = 23.6$ (Paper I), the companion is likely a very faint MS star.

3.4.7 Source W15

Of the 10 additional X-ray sources detected by Zhao et al. (2020), three are in our FUV field of view: W15, W16 and W17. Three ultraviolet sources are detected within the error circle of W15: two MS stars, ID449 and ID452, and a gap source, ID912. The number of chance coincidences of MS stars in the error radius for W15 is 0.845 but for a gap source is only 0.068, meaning that the gap source is the more likely true counterpart. The gap object is also the closest to W15 at a distance of $0.109''$ and corresponds in position to the optical counterpart for W15 proposed by Zhao et al. (2020), who confirmed that it is a cluster member with a probability of 96.7% (Piotto et al. 2015; Nardiello et al. 2018) and that this source has a blue excess in ultraviolet to infrared wavelengths, thus concluding that W15 is a CV. This source was not in the Guhathakurta et al. (1998) catalogue, but due to its location blueward of the MS in the $FUV - UV$ CMD and its proximity to W15, we agree that ID912 is most likely a CV.

3.4.8 Source W16

Zhao et al. (2020) suggest a sub-subgiant as a companion to W16 which correlates to the position of ID1029, a source that is located just below the red giant branch in both the $FUV - UV$ and optical CMDs in this work. At a distance of $0.108''$ from W16, it is the only source detected in the FUV to be within the error circle of X-ray source W16. As Göttgens et al. (2019) find variable $H\alpha$ emission from this source using MUSE, Zhao et al. (2020) propose that this is an RS CVn type of AB. The FUV light curve for ID1029 illustrated in Sect. 4 shows that it is not more variable relative to other sources with similar FUV magnitudes (Fig. 6).

3.4.9 Source W17

Only one source was found within the error circle for W17, ID1681, another source with an FUV detection but no counterpart in the UV , however it does have a counterpart from the optical catalogue (Guhathakurta et al. 1998, their source #3175); a star located blueward of the MS in the optical CMD. Piotto et al. (2015) and Nardiello et al. (2018) also find a source at this position with a cluster membership probability of 98.1%. Zhao et al. (2020) proposed two potential counterparts to W17, both MS stars which exhibited brightness variability, neither of which match to the position of ID1681. The light

curve for ID1681 is shown in Fig. 8, which only shows a slight variation in magnitude.

3.4.10 MSP A

Two MSPs were found in M30 by Ransom et al. (2004) using radio pulsar timing, one of which (PSR J2140–2310A, MSP A) was also faintly observed in X-ray wavelengths by Ransom et al. (2004) and is detected again by Zhao et al. (2020) who measure a higher number of X-ray counts for MSP A. Ransom et al. (2004) suggest a MS star companion within $0.09''$ of this pulsar that was seen in V_{555} images but not U_{336} or I_{814} images. This companion is not seen in our ultraviolet exposures, instead the only source within the error circle is a red giant, ID1217, located just off the MS turnoff, and at $0.399''$ away from the position of MSP A, is likely to be a chance superposition.

4 VARIABLE FUV SOURCES

In order to find objects in the FUV dataset that exhibit significant variability, we plot the standard deviation σ_{mean} of the FUV magnitude over the mean FUV magnitude for each star (Fig. 6). Variable sources have a larger deviation than other sources with the same magnitude and the red line in the figure indicates twenty percent above the binned average σ_{mean} as a rough criterion for variability. From this, seven BS, four HB, five RGB and one WD/Gap source are identified as variable, and their light curves are plotted in Fig. 7. The two WD/Gap sources ID350 and ID1230 are also included as they are close to the variability criterion. Also included in Figs. 6 & 7 are the Gap source ID912 and the RGB stars ID181 and ID1029 as these are potential X-ray counterparts. The light curves for the three sources within X-ray source error circles that are detected in the FUV but with no UV counterparts are given in Fig. 8. The light curves for 28 MS stars is shown in Fig. A1 in the Appendix. The other sources above the variability criterion that are not identified were unremarkable in their light curves. The cluster membership probabilities for some of the sources discussed are given in Table 2 (Piotto et al. 2015; Nardiello et al. 2018).

The periods of variable objects can be estimated by producing Lomb–Scargle periodograms (Lomb 1976; Scargle 1982) which performs a Fourier transform of the light curve data points. In order to check for discrepancies in the data due to the observing window used, the window function is also calculated from a Lomb–Scargle periodogram with a non-floating mean model and without centering the data (VanderPlas 2018). The window function is plotted over the periodograms in Fig. A2 in the Appendix. The accuracy of this period is checked by comparing to the folded light curves. Four of our variable sources have periods measured and these are then used to plot sine curves representing this periodicity onto the light curves. The photometric properties and any found periods are given in Table A1 in the Appendix for all variable sources. The uncertainties in the FUV_{mean} magnitudes are larger than those for the $FUV - UV$ measurements since they are taken from the individual flat fielded exposures rather than the cleaner drizzled master image.

4.1 Blue stragglers

The light curves of the BS stars are shown in Fig. 7. The source ID267 corresponds within $0.07''$ to the position of the variable M30_5 identified as a W UMa-type contact binary by Pietrukowicz & Kaluzny (2004) who measure a period of 7.61 hours. Due to the symmetry

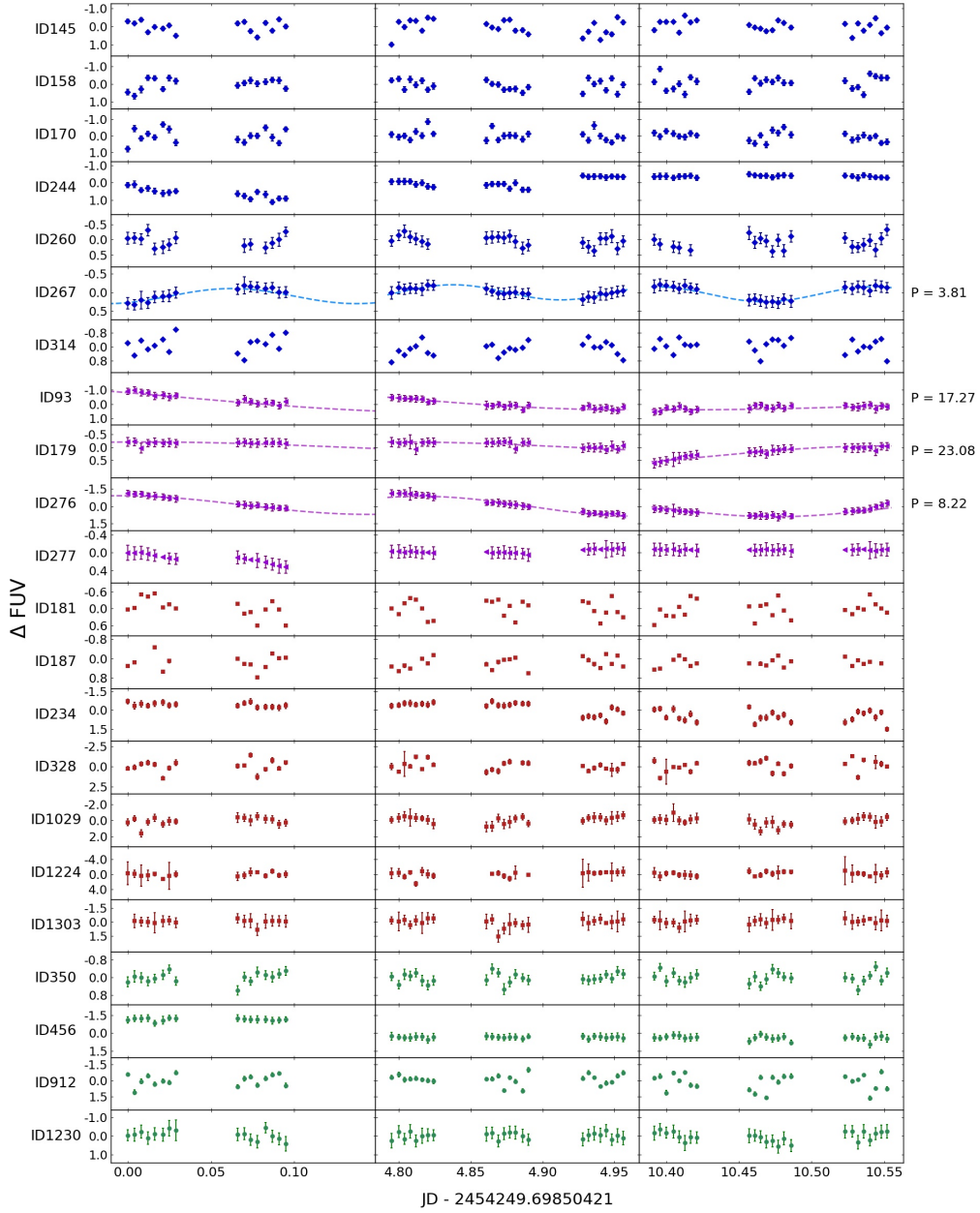


Figure 7. *FUV* mean-subtracted magnitudes ($\Delta FUV = FUV - FUV_{mean}$) are plotted over time for seven variable BS sources (blue diamonds), four HB stars (ID93 - ID277, purple triangles), seven RGB stars (red squares) and four gap objects (green circles). The sine curves represent the periods which are found for several sources, and the period in hours is given. The measured period of 3.81 hours for ID267 is half of the true period for this contact binary (see text).

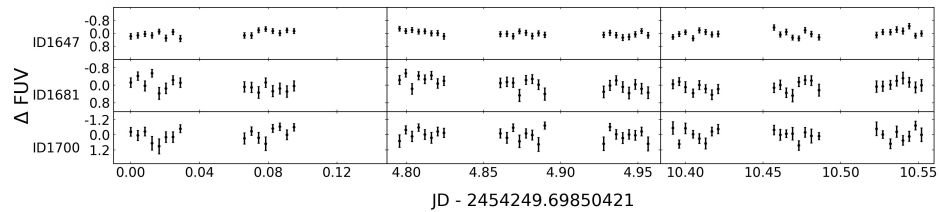


Figure 8. *FUV* light curves for the three potential X-ray counterparts that have no matching *UV* measurement. The mean-subtracted magnitude is plotted over time.

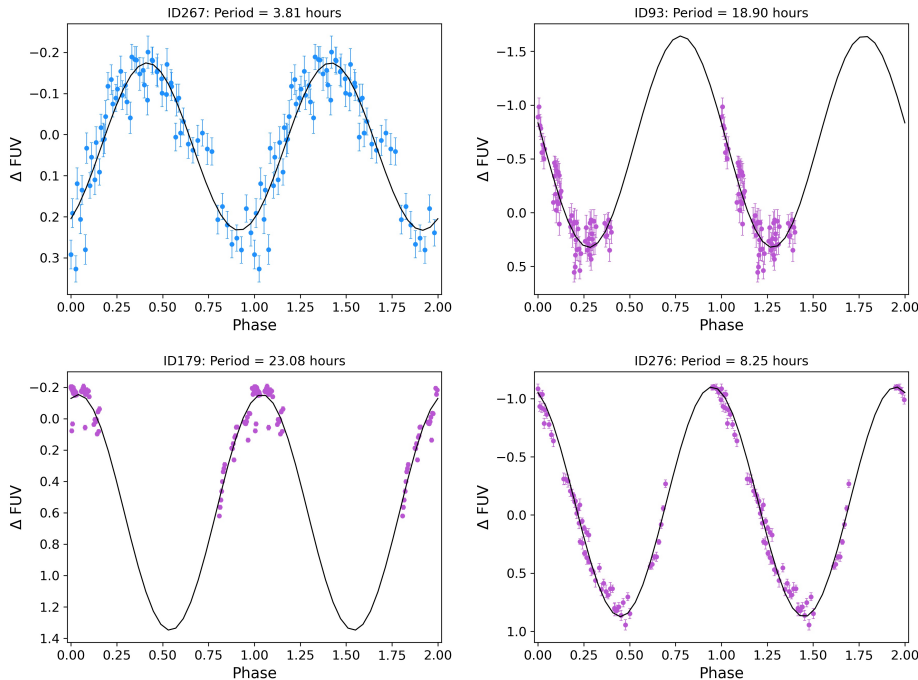


Figure 9. Folded light curves for the BS and HB stars with estimated periods shown in Fig. 7. The measured period of 3.81 hours for ID267 is half of the true period for this contact binary (see text)

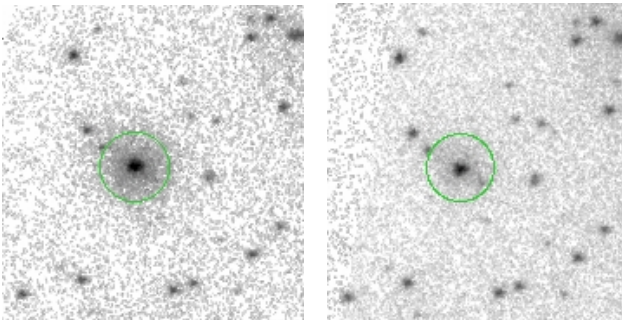


Figure 10. *FUV* image of the CV candidate ID456 during dwarf nova outburst (left) and quiescence (right).

indicate starspot activity (Brown et al. 2011). Some stars show little variance in magnitude over the course of one observing day, and then have large variations on another day, for example sources ID268 and ID1226 (this behaviour was also seen in the RGB star ID234). ID1226 has one of the highest σ_{mean} values and remains stable for almost two observing epochs and then exhibits a period of large variability before settling into a stable period again.

Source ID806 is on the edge of the error circle for X-ray source A3, and whilst it shows slight fluctuations in *FUV* magnitude, its σ_{mean} is no larger than sources of similar magnitude, and it remains likely that one of the RGB stars is the likely counterpart to A3.

5 SUMMARY

We performed a comparison of the positions of the sources detected in the far-ultraviolet to known X-ray sources and possible companions or counterparts to these were discussed. The crowding in the centre

of the cluster makes it difficult to determine the exact counterparts, and in this work all those that are within the 95% error radii of the X-ray source are considered. Out of the ten X-ray sources within our field of view, six confident counterparts are: the RGB star with strong *FUV* emission ID283 to X-ray source A2, the gap source ID456 to source C, agreeing with Luger et al. (2007) that this is a CV, gap source ID912 to X-ray source W15, agreeing with Zhao et al. (2020) that this is also a CV, RGB star ID1029 to W16 which was proposed by Zhao et al. (2020) to be a RS CVn, and the two sources detected in the *FUV* but with no matching *UV* counterparts: ID1647 to X-ray source B and ID1700 to source 6. Although MS stars are much more numerous in the core region of globular clusters, if we include ID187 as the possible counterpart to A3, then three of the counterparts to the ten X-ray sources are red giants.

Light curves were shown for *FUV*-variable objects and we found periods for four of these sources. Several of these variables were considered as potential X-ray counterparts. Out of the seven variable BS stars, the half-period is measured for one of them that is a known W UMa-type contact binary. Four HB stars show variability, two are known RR Lyrae variables and one (ID179) is potentially a new RR Lyrae (RRab) classification, however it may be a field star. One gap source, ID456, a previously identified CV, shows a dwarf nova event and two other gap sources have weak variability. Twenty-eight MS stars also exhibit fluctuations.

Observations into the far-ultraviolet allow us to detect and identify exotic stellar systems such as CVs which are less easily observed at optical wavelengths amongst the numerous optically-bright MS stars. Studies using ultraviolet wavelengths and multi-wavelength comparisons continue to provide valuable insights into the different populations in dense stellar systems.

DATA AVAILABILITY

The data underlying this article are available in the Mikulski Archive for Space Telescopes (MAST): <https://archive.stsci.edu>. The datasets are derived from images in the public domain: https://archive.stsci.edu/proposal_search.php?mission=hst&id=10561. The catalogue of sources is available at CDS via anonymous ftp to cdsarc.u-strasbg.fr (130.79.128.5) or via the VizieR catalogue access tool (Ochsenbein et al. 2000) at: <http://vizier.u-strasbg.fr/viz-bin/VizieR?-source=J/MNRAS/511/3785>. This research also made use of optical data also available at CDS: <https://cdsarc.cds.unistra.fr/viz-bin/cat/J/AJ/116/1757>.

This paper has been typeset from a $\text{\TeX}/\text{\LaTeX}$ file prepared by the author.

ACKNOWLEDGEMENTS

We thank the referee for the detailed and thoughtful comments. PK acknowledges support from the Grant Agency of the Czech Republic under grant number 20-21855S.

REFERENCES

- Bacon R., et al., 2017, *A&A*, 608, A1
 Bailey S., 1902, Annals of Harvard College Observatory, 38, 1
 Brown A., et al., 2011, *Proc IAU*, 273, 78
 Echiburú C. S., Guillot S., Zhao Y., Heinke C. O., Özel F., Webb N. A., 2020, *MNRAS*, 495, 4508
 Edmonds P. D., Gilliland R. L., Heinke C. O., Grindlay J. E., 2003, *ApJ*, 596, 1177
 Göttgens F., et al., 2019, *A&A*, 631, A118
 Greenfield P., White R. L., 2000, *ASPCS*, 216, 59
 Guhathakurta P., Webster Z. T., Yanny B., Schneider D. P., Bahcall J. N., 1998, *AJ*, 116, 1757
 Harris W. E., 1996, *AJ*, 112, 1487
 Harris W. E., 2010, A New Catalog of Globular Clusters in the Milky Way ([arXiv:1012.3224](https://arxiv.org/abs/1012.3224))
 Hills J. G., Day C. A., 1976, *Astrophys. Lett.*, 17, 87
 Hong J., van den Berg M., Schlegel E. M., Grindlay J. E., Koenig X., Laycock S., Zhao P., 2005, *ApJ*, 635, 907
 Hong J., Vesperini E., Belloni D., Giersz M., 2016, *MNRAS*, 464, 2511
 Ivanova N., Heinke C. O., Rasio F. A., Belczynski K., Fregeau J. M., 2008, *MNRAS*, 386, 553
 Kains, N. et al., 2013, *A&A*, 555, A36
 Lomb N. R., 1976, *Ap&SS*, 39, 447
 Lugger P. M., Cohn H. N., Heinke C. O., Grindlay J. E., Edmonds P. D., 2007, *ApJ*, 657, 286
 Mansfield S., Dieball A., Kroupa P., Knigge C., Zurek D. R., Shara M., Long K. S., 2022, *MNRAS*, 511, 3785
 McCrea W. H., 1964, *MNRAS*, 128, 147
 Nardiello D., et al., 2018, *MNRAS*, 481, 3382
 Ochsenbein et al., 2000, The VizieR database of astronomical catalogues, [doi:10.26093/cds/vizieR](https://doi.org/10.26093/cds/vizieR)
 Pietrukowicz P., Kaluzny J., 2004, *Acta Astron.*, 54, 19
 Piotto G., et al., 2015, *The Astronomical Journal*, 149, 91
 Ransom S. M., Stairs I. H., Backer D. C., Greenhill L. J., Bassa C. G., Hessels J. W. T., Kaspi V. M., 2004, *ApJ*, 604, 328
 Scargle J. D., 1982, *ApJ*, 263, 835
 Shara M. M., Hurley J. R., 2006, *ApJ*, 646, 464
 Smith H., 1995, *RR Lyrae Stars*. Cambridge University Press, Cambridge UK
 Stetson P. B., 1987, *PASP*, 99, 191
 VanderPlas J. T., 2018, *ApJS*, 236, 16

- Zhao Y., et al., 2020, *MNRAS*, 499, 3338
 Zurek D. R., Knigge C., Maccarone T. J., Pooley D., Dieball A., Long K. S., Shara M., Sarajedini A., 2016, *MNRAS*, 460, 3660

APPENDIX

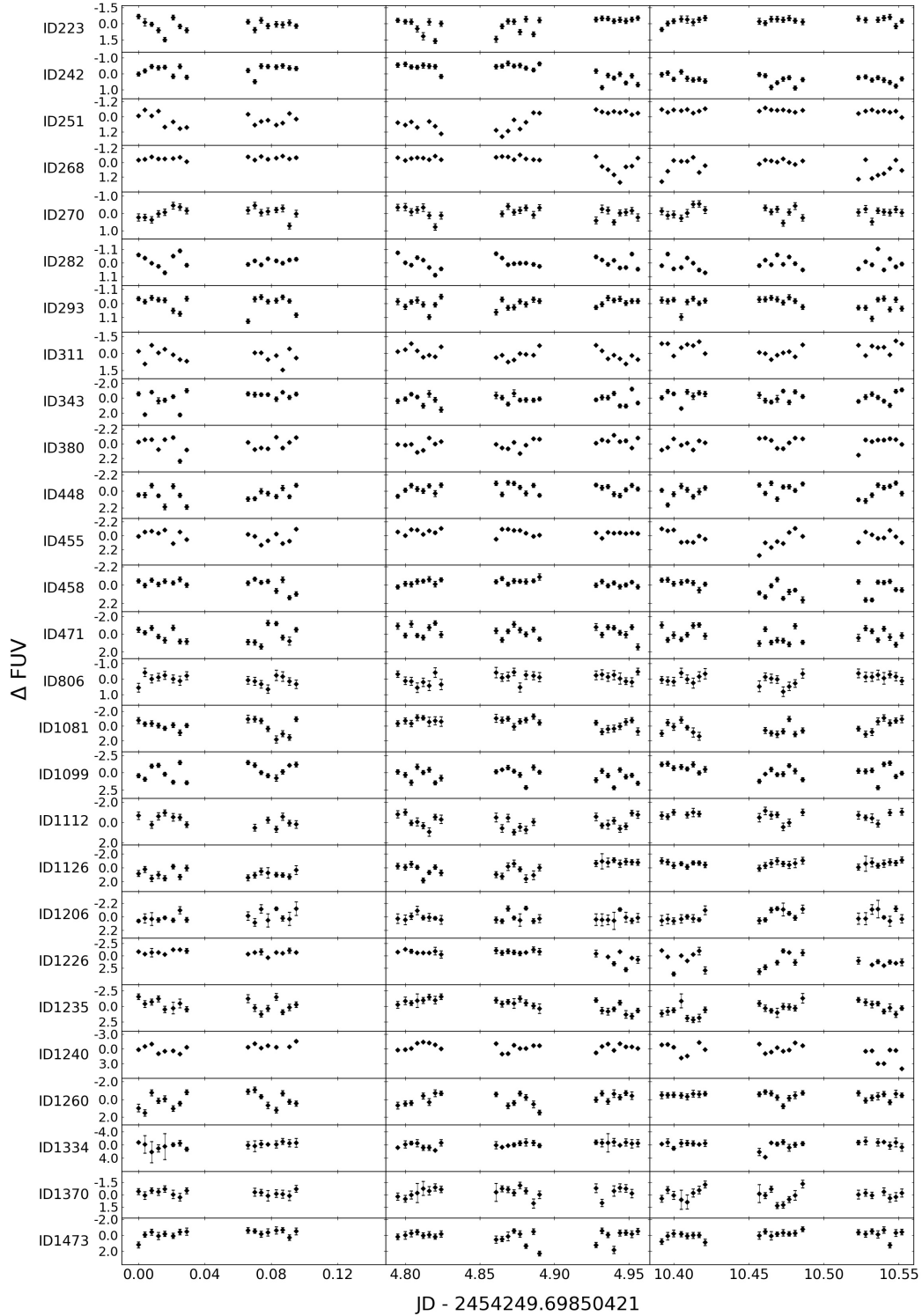


Figure A1. Light curves for the 28 MS stars which showed variability.

Table A1. Photometric and variability parameters of all variable sources whose light curves are shown in this work.

ID	Type	$FUV - UV$ [mag]	FUV_{mean} [mag]	σ_{mean}	Period [hours]
93	HB	3.870 ± 0.011	20.518 ± 0.099	0.368	17.27
145	BS	1.961 ± 0.030	21.050 ± 0.152	0.344	
158	BS	1.923 ± 0.037	21.146 ± 0.161	0.331	
170	BS	2.054 ± 0.034	21.091 ± 0.158	0.309	
179	HB	0.234 ± 0.002	16.103 ± 0.013	0.212	23.08
181	RG	5.677 ± 0.068	22.726 ± 0.274	0.302	
187	RG	3.971 ± 0.037	21.690 ± 0.172	0.469	
223	MS	3.215 ± 0.091	21.658 ± 0.226	0.593	
234	RG	5.176 ± 0.044	21.455 ± 0.196	0.556	
242	MS	2.688 ± 0.052	21.340 ± 0.181	0.437	
251	MS	2.715 ± 0.058	21.581 ± 0.221	0.585	
260	BS	2.098 ± 0.043	20.835 ± 0.162	0.310	
267	BS	0.176 ± 0.007	17.999 ± 0.034	0.149	3.81
268	MS	3.175 ± 0.050	21.703 ± 0.229	0.571	
270	MS	2.495 ± 0.062	21.288 ± 0.170	0.416	
276	HB	1.857 ± 0.005	18.401 ± 0.038	0.638	8.22
277	HB	0.332 ± 0.002	15.989 ± 0.012	0.097	
282	MS	2.536 ± 0.032	21.862 ± 0.278	0.450	
293	MS	2.697 ± 0.046	21.585 ± 0.205	0.446	
311	MS	3.413 ± 0.056	22.200 ± 0.403	0.708	
314	BS	2.046 ± 0.092	21.390 ± 0.373	0.412	
343	MS	3.048 ± 0.066	22.120 ± 0.357	0.740	
350	Gap	-1.864 ± 0.098	21.238 ± 0.169	0.231	
380	MS	3.522 ± 0.038	23.109 ± 0.346	0.771	
448	MS	3.438 ± 0.038	23.462 ± 0.409	0.795	
455	MS	3.793 ± 0.038	23.552 ± 0.433	0.867	
456	Gap	0.821 ± 0.019	20.443 ± 0.099	0.675	
458	MS	3.706 ± 0.037	23.317 ± 0.377	0.693	
471	MS	3.513 ± 0.041	23.603 ± 0.430	0.753	
806	MS	3.801 ± 0.059	22.792 ± 0.282	0.303	
912	Gap	2.233 ± 0.093	24.019 ± 0.512	0.603	
1029	RG	3.929 ± 0.064	23.817 ± 0.429	0.468	
1081	MS	3.507 ± 0.041	23.753 ± 0.473	0.874	
1099	MS	4.067 ± 0.064	24.187 ± 0.486	0.944	
1112	MS	3.756 ± 0.036	23.513 ± 0.423	0.843	
1126	MS	3.732 ± 0.047	23.469 ± 0.412	0.830	
1206	MS	2.937 ± 0.049	21.309 ± 0.149	0.746	
1224	RG	4.074 ± 0.057	22.524 ± 0.471	0.597	
1226	MS	2.491 ± 0.064	21.992 ± 0.556	1.437	
1230	Gap	0.539 ± 0.054	21.333 ± 0.147	0.227	
1235	MS	3.682 ± 0.055	24.143 ± 0.570	0.924	
1240	MS	4.041 ± 0.065	24.577 ± 0.712	1.088	
1260	MS	3.903 ± 0.065	22.847 ± 0.312	0.817	
1303	RG	3.412 ± 0.036	21.391 ± 0.176	0.388	
1334	MS	3.937 ± 0.053	23.484 ± 0.422	0.900	
1370	MS	4.104 ± 0.070	23.560 ± 0.433	0.801	
1473	MS	3.573 ± 0.051	22.942 ± 0.314	0.613	

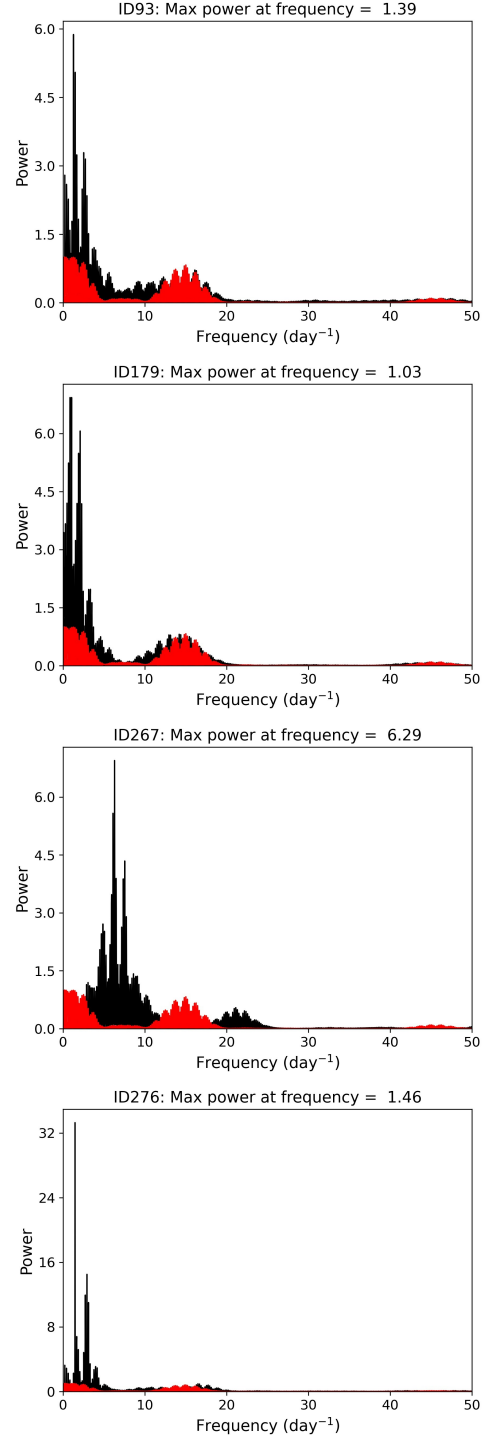


Figure A2. Lomb–Scargle periodograms (black) of the sources with periods measured along with the window function plotted in red.